

Madhavi Krishnan

CONTROL, MANIPULATION AND MEASUREMENT OF MATTER AT THE MOLECULAR SCALE

The desire to freely suspend the constituents of matter in order to study their behaviour can be traced back over 200 years to the diaries of Lichtenberg. From radio-frequency ion traps to optical tweezing of colloidal particles, existing methods to trap matter in free space or solution rely on the use of external fields that often strongly perturb the integrity of a macromolecule in solution. Recently, we introduced the electrostatic fluidic trap, a field-free principle that supports stable, non-destructive confinement of single macromolecules in room temperature fluids, representing a paradigm shift in a nearly century-old field. The spatio-temporal dynamics of a single electrostatically trapped molecule reveals fundamental information on its properties, e.g., size and electrical charge. We have recently developed the ability to measure the electrical charge of a single macromolecule in solution with a precision much better than a single elementary charge. Since the electrical charge of a macromolecule in solution is in turn a strong function of its 3D conformation, our approach enables for the first time precise, general measurements of the relationship between 3D structure and electrical charge of a single macromolecule, in real time. In a related sphere of activity we use external electrical and optical forces in conjunction with our trap in order to achieve digital functionalities such as data storage and signal gating in a single levitating colloidal particle. In this Article we provide an overview of key experiments and advances in this emerging area of single particle/molecule science and briefly discuss prospects for future research.

The ability to trap an object in space, whether a single atom or a macroscopic entity, is of primary importance in fields ranging from quantum optics^[1] to soft condensed matter physics, biophysics, and clinical medicine^[2]. Many sophisticated methodologies have been developed to counter the randomizing effect of Brownian motion in solution^[3-10], but stable trapping of nanometric objects remains challenging^[8-10]. For example, traditional optical tweezing relies on the polarizability of the object of interest. Since polarizability scales as the volume of the particle the approach rapidly loses efficacy with decreasing object size and is unsuitable for manipulating small macromolecules. More recently, traps exploiting the optical near-field in plasmonic nanostructures have achieved the ability to spatially

confine single macromolecules^[10, 11]. However the interaction of strong local electromagnetic fields with a soft, deformable entity such as a macromolecule causes unfolding and structural deformation of the object of interest.

Our electrostatic trap concept is free of externally applied fields and provides trapping and levitation of single charged nanoscale particles and biological macromolecules on time-scales on the order of an hour^[12]. The principle is based on the spatial modulation of the electrostatic interaction energy created in a topographically-tailored fluidic nanoslit (Fig. 1a). As a result, the trap requires no external intervention and is free of constraints imposed by the object's mass or dielectric function. The stiffness and stability of the trap can be tuned by varying the geometry of the system and the ionic strength of the solution (Fig. 2). Furthermore, the technique may be readily integrated with other manipulation mechanisms. For example, combining external electric and optical fields with a bistable potential well for a plasmonic nanorod we have demonstrated the ability to write, store and read out binary states and gate optical signals using a single nanoparticle in solution (Figs. 3 and 4)^[13]. Very recently we have achieved the ability to perform high precision ($< 1 e$) electrical measurements on single trapped molecules such as nucleic acids, and globular and intrinsically disordered proteins in solution (Figs. 5 and 6)^[14]. Operating in the weak trapping regime where residence times are small, we measure the average escape time of single trapped molecules, which gives a very precise measure of the depth of the trap and therefore the molecule's effective charge. The measurement also facilitates an estimate of a dielectric coefficient of the molecular interior, and can be performed in real-time (Fig. 7). Since macromolecular charge strongly depends on 3D conformation, high precision electrometry offers a new approach to probe structure, fluctuations, and interactions of a single molecule in solution, likely opening up an unexplored physical dimension in biomolecular measurement.

SPATIAL CONTROL OF SINGLE NANOMETER-SCALE ENTITIES IN THE FLUID PHASE

Principle of the electrostatic fluidic trap for nanoscale matter in solution

Unlike traditional external field-based approaches to spatially control matter, our approach relies on equilibrium thermodynamics to trap molecular scale matter in solution. Specifically we exploit the electrostatic interaction between a charged

Prof. Dr. Madhavi Krishnan
University of Zurich
Department of Chemistry & Department of Physics
Winterthurerstrasse 190, CH 8057 Zurich, Switzerland
Phone: +41 44 635 44 65
E-Mail: madhavi.krishnan@uzh.ch

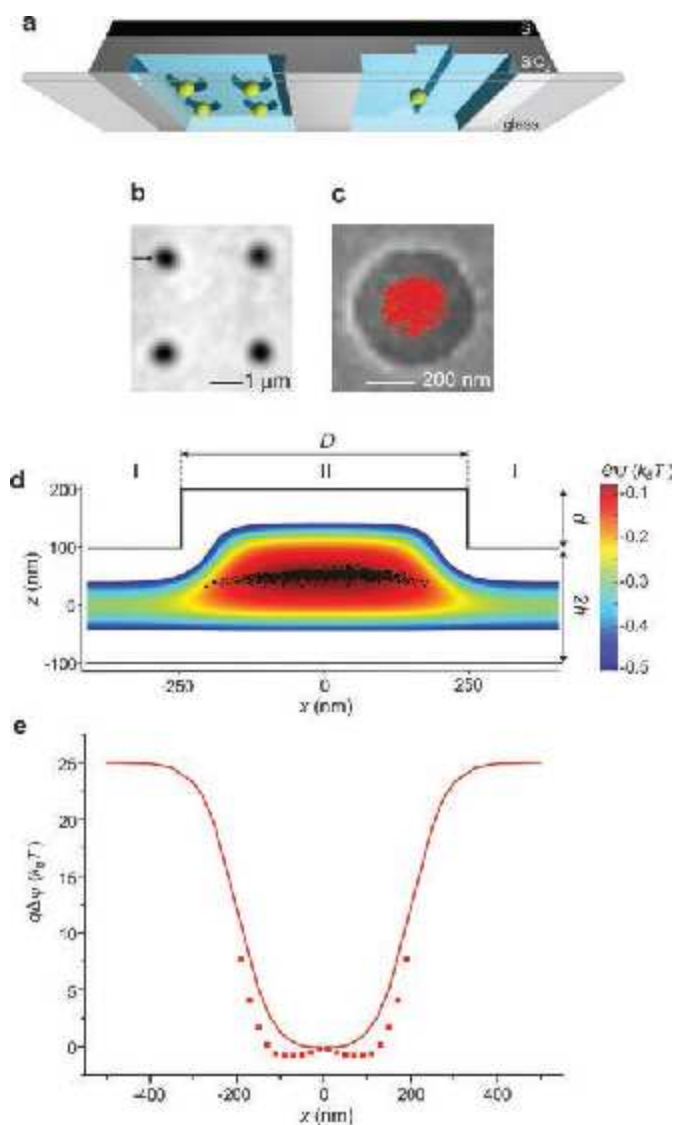


Fig. 1: Pictorial representation of the experiment and illustration of the electrostatic trap principle. (a) Illustration of an electrostatic fluidic trap device with nanostructured slit surfaces. (b) Scattering interferometric (iSCAT) image of 4 gold nanoparticles 100 nm in diameter confined by axially symmetric surface indentations or pocket nanostructures. Destructive interference between the light scattered by the particle and that reflected from the substrate causes the particle to appear dark against a light background. (c) Trajectory of a single particle overlaid on an SEM of the underlying surface topography (d) Calculated electrostatic interaction energy landscape in the slit for a unit positive charge, using typical experimental parameters. Geometric parameters that are important in the confinement interaction are highlighted: slit height, $2h$; surface nanostructure diameter or width, D ; nanostructure depth, d . The bottom (region I) and shoulders (region II) of the potential well are also shown. Superimposed on the potential landscape is a scatter plot of particle positions in the axial (z) dimension measured using scattering interferometry (black). (e) Axial minimum energy profile across the trap for a particle of charge $q = -120 e$. The red symbols denote values of local interaction energy inferred from experimentally measured scatter plots.

object and a like-charged wall in an electrolyte. In our experiments, the charge on the slit walls and the particles or molecules arises from the spontaneous ionization of surface chemical groups upon contact with water^[15]. Consider a charged object in solution confined between two parallel plates carrying a surface charge of the same sign. It is well known that the electrostatic potential near an isolated glass or SiO₂ surface, ψ decays exponentially away from the surface value, ψ_0 as: $\psi(z) = \psi_0 e^{-\kappa z}$, where κ^{-1} is the Debye length and for a monovalent

electrolyte may be given in nanometers by $0.3/\sqrt{C}$, where C is the salt concentration in solution in mol/L^[16]. Two charged planes separated by a gap of height, $2h$ in a fluid thus give rise to an electrostatic potential minimum midway between them. For low values of ψ_0 , the potential at the midplane due to both surfaces can be taken to be simply additive and is given by $\psi_m = 2\psi_0 e^{-\kappa h}$ (region I in Fig. 1d). An indentation in the surface that locally increases the gap height by d would give rise to a corresponding potential minimum of $\psi_m = 2\psi_0 e^{-\kappa(h+d/2)}$ (region II in Fig. 1d). So a unit positive charge traversing a width modulation in the gap would experience a change in electrostatic energy given by $\Delta\psi = 2\psi_0 e^{-\kappa h} (1 - e^{-\kappa d/2})$. When $d \rightarrow 0$, i.e., the height modulation vanishes, the slit consists of two flat parallel walls facing each other, and $\Delta\psi \rightarrow 0$. For large κd , on the other hand, $\Delta\psi \approx \psi_m = 2\psi_0 e^{-\kappa h}$. Thus for a particle of charge q , the geometric modulation of the gap height creates a modulation in interaction energy of $q\Delta\psi$ in the plane of the slit. Since the surface potential, ψ_0 of typical charged oxide surfaces in solution is of the order of 100 mV, it is clear that well depths of several $k_B T$ should be easily within reach of this principle (25 mV corresponds to approximately $1 k_B T$ in interaction energy for a unit charge at room temperature). If $q\Delta\psi$ is substantially larger than the thermal energy $k_B T$, the particle is stably trapped for a period given by a Kramers-type expression^[17],

$$\tau = \tau_0 \exp\left(\frac{q\Delta\psi}{k_B T}\right).$$

Here τ_0 is given by the time that a free particle would take to diffuse across a distance corresponding to the width of the potential well in the absence of the trap^[18], which in general may be estimated as the radius of the surface indentation. Such a thermodynamic potential well should thus be capable of confining a charge object for extended periods without the use of any external fields. Note that values of $q\Delta\psi \approx 10k_B T$ over a range of 200 nm suggests spatial confinement on length scales comparable with a diffraction limited optical focus, on time scales of the order of 10 s for a single macromolecule of hydrodynamic radius, 2.5 nm.

While these simple considerations based on the linearization of the governing equations, valid for low surface potentials or far away from surfaces are not quantitatively exact, they give a physical picture of how geometrical modulation of a gap can translate to a modulation of the electrostatic potential in a fluid. They also furnish key insight into optimal design of electrostatic landscapes to trap and manipulate single charged particles in fluids. Accordingly, systems with small values of κh and walls with a high surface potential, ψ_0 would be expected to work best in creating deep local potential wells, capable of retaining a charged object for a long time. Furthermore under a given set of conditions, i.e. ionic strength and slit depth, the shape and depth of a potential well can be tailored using the geometry of the surface indentation (Fig. 2). In our original demonstration of the experimental feasibility of the concept we presented stable trapping of charged nanospheres as small as 20 nm polystyrene and 50 nm lipid vesicles in water^[12]. Later we described how spatial mapping of potential wells can be used in conjunction with free energy calculations^[19] to directly measure the charge of single trapped objects in a highly parallel fashion^[20].

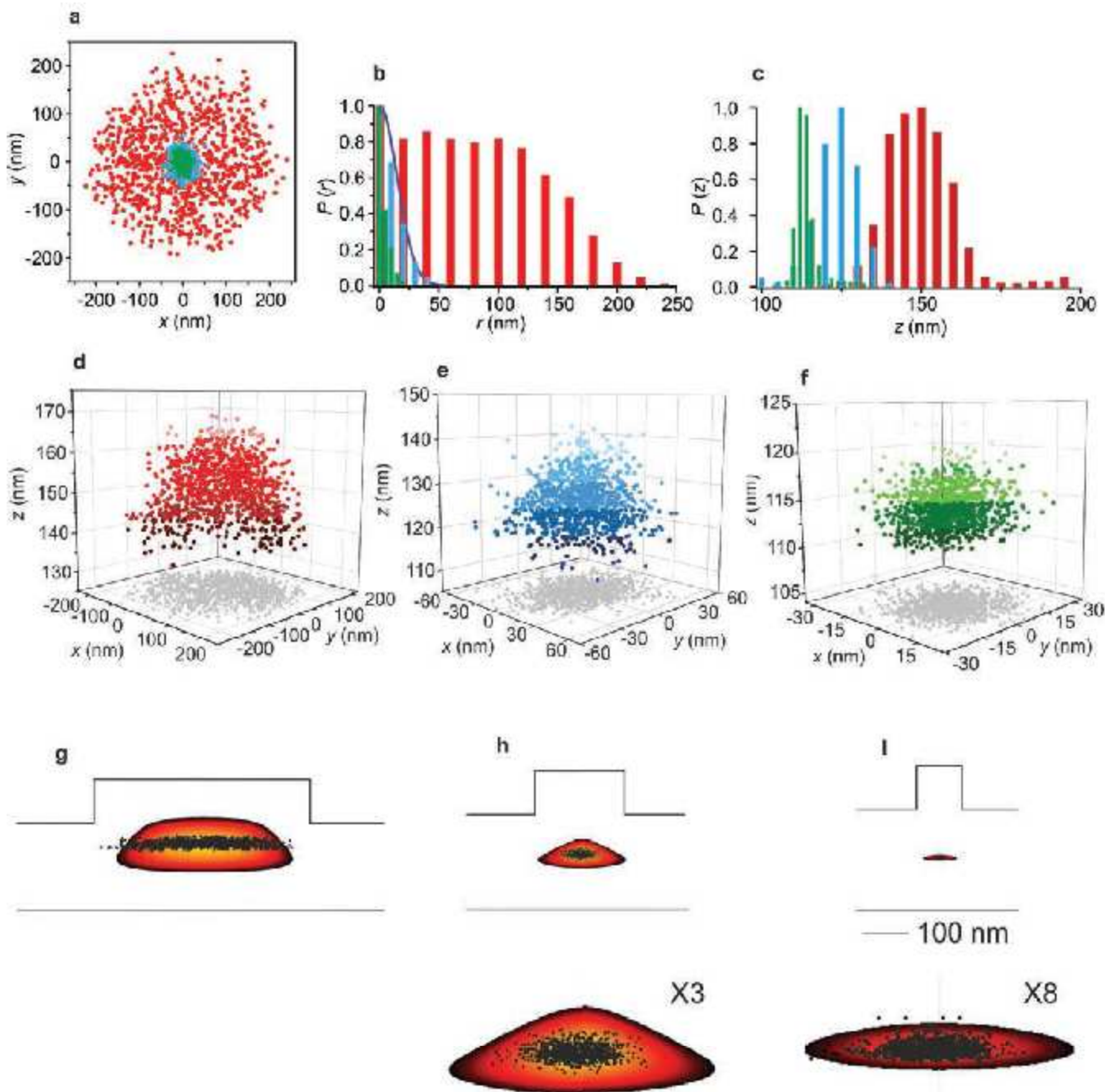


Fig. 2: Electrostatically trapped gold nanospheres studied using scattering interferometric imaging. (a) Scatter plots of trapped particle positions for lateral motion of representative 80 nm gold particles trapped by $D= 500$ nm (red), 200 nm (blue), and 100 nm (green) pockets acquired using iSCAT imaging with an exposure time of 1 ms. (b) Averaged radial and (c) axial probability density distributions obtained by tracking an ensemble of particles trapped by the three pocket geometries. (d), (e), (f) 3D scatter plots of representative particles trapped in the three geometries and (g), (h), (i) their overlay on the corresponding calculated electrostatic potential distribution. The panels under (h) and (i) represent the same plots magnified 3 and 8 times respectively. The electrostatic potential is presented on a linear color scale going from high (black) to low energy (yellow) for a unit negative charge. For emphasis, only the minimum of the well is shown.

The experiments are typically performed using pM concentrations of particles or molecules in solutions with salt concentrations in the range 0.05 to 2 mM monovalent salt. Particles are initially introduced into the slit by capillary flow, but observed under purely diffusive conditions using optical microscopy. In general we use scattering interferometry^[21] (iSCAT) for large (ca. 100 nm diameter), strongly scattering particles (Figs. 1-4), and wide-field fluorescence microscopy for weakly emitting, fluorescently labelled macromolecules (Figs. 5-7).

MANIPULATING A SINGLE LEVITATING COLLOIDAL PARTICLE TO ACHIEVE DIGITAL FUNCTIONALITIES IN THE FLUID PHASE

The binary switch is a basic component of digital information. From phase change alloys to nanomechanical beams, molecules and atoms, new strategies for controlled bistability hold great interest for emerging technologies. Current approaches to controlled bistability are mostly based on the solid state, where response times are small, but often require high ener-

gies, ultra-cold temperatures, or face challenges in integration and parallelization^[22-27]. Fluids in comparison mediate intermolecular interactions in matter at room temperature, while permitting relatively low-friction, rapid responses to external fields. Thus photonic, logic and rudimentary computing capabilities have been demonstrated in bulk suspension^[28-32]. Yet devices that harness the properties of isolated mesoscopic entities in solution remain elusive.

We have exploited our ability to exert precise spatiotemporal control on nanometre-scale matter in a fluid, to realize digital functionalities such as switching, gating and data storage in a single colloid, with further implications for signal amplification and logic operations. This fluid-phase bit can be arrayed at high densities, manipulated by either electrical or optical fields, supports low-energy, high-speed operation and marks a first step toward colloidal information .

A bistable levitating colloidal particle for information storage and signal gating

In order to illustrate our ability to write, store and read-out information, as well as to switch and gate signals, using a single nanometer-scale particle stably levitated in a fluid we used single nanorods confined in angular double-well potentials. These potential wells were created using an orthogonal arrangement of cigar-shaped wells as shown in Figs. 3a and b. The symmetry-axis of the T-geometry effectively offers a trapped object a single spatial degree of freedom with a free energy barrier in between that the particle attempts to traverse, only to be trapped in the neighbouring minimum if it does succeed. While both states are equally populated at equilibrium (histogram in Fig. 3d), for large barriers, $B > 20 k_B T$ the object is kinetically trapped in one of two spatial states. Furthermore, on account of the morphology of the minima, transition of a rod-shaped particle across the barrier is also accompanied by a rotation through $\pi/2$ in the plane

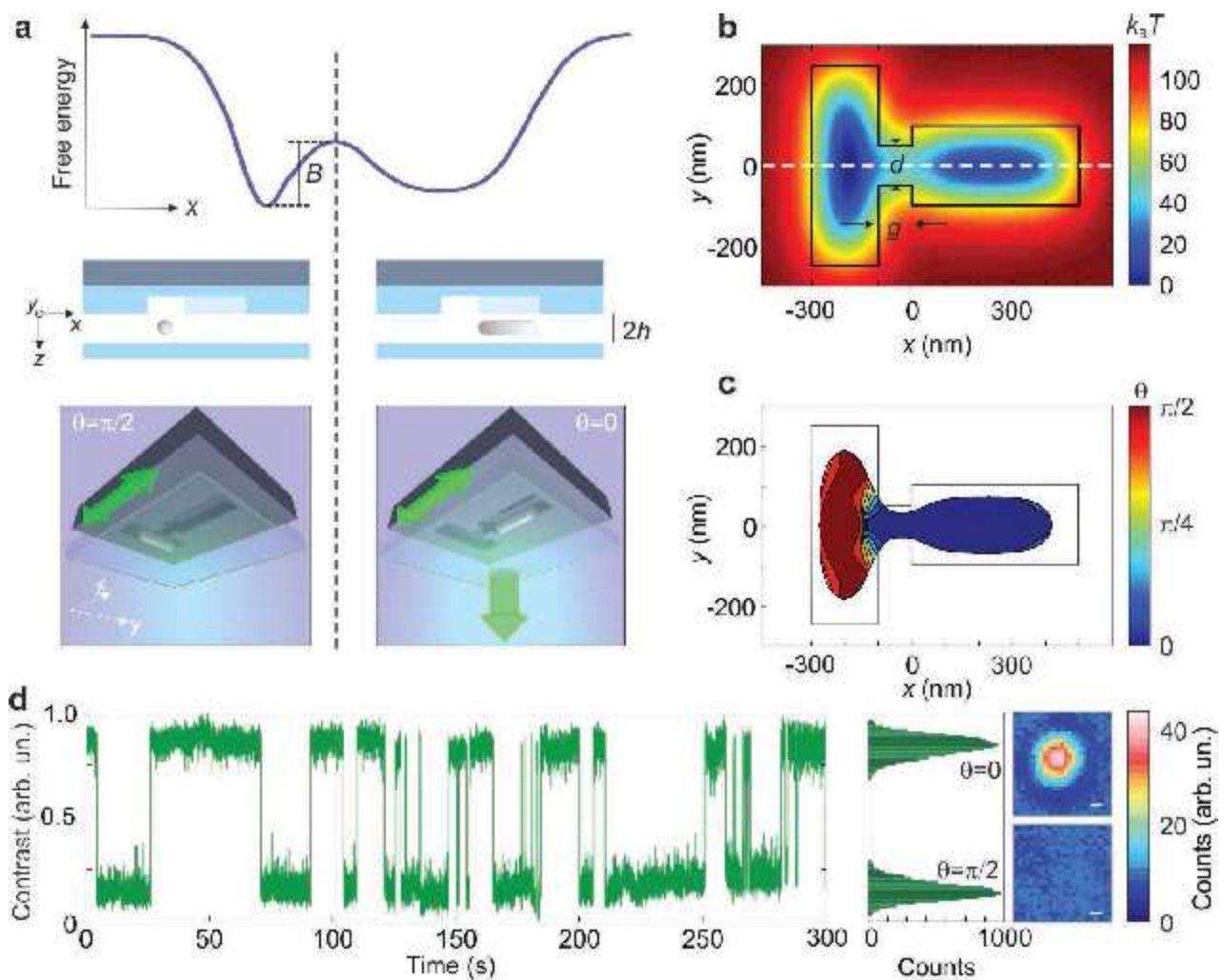


Fig. 3: A bistable colloidal particle the first step towards information storage and read-out in the fluid phase. (a) Cross-section and 3D illustration of a single nanorod trapped in either of two angular states $\theta = \pi/2$ (left) and 0 (right) - in a parallel-plate fluidic nanostructure. $2h$ represents the height of the slit. The line profile of rod free energy (top) along the dotted line in (b) illustrates the bistable electrostatic potential with a barrier of height, B created by the T-shaped surface topography. (b) Calculated xy distribution of minimum axial (z) and angular electrostatic energy for a negatively charged nanorod (net charge, $-250 e$) trapped in the bistable well. The height of the barrier is tailored using the geometry of the T-intersection. Here, $g = d = 100$ nm and $2h = 180$ nm. Throughout this work we approximate the system's electrical free energy by the electrostatic energy of the rod. (c) 2D Plot of the most probable rod angle, θ in the xy plane. The two spatial free energy minima clearly correspond to mutually perpendicular orientations of the rod. (d) Time-trace of normalized optical contrast for a nanorod trapped in a bistable well with an estimated barrier height, $B \sim 10 k_B T$. The electrostatic pixel (bistable nanorod) is illuminated with a linearly polarized probe beam parallel to one arm of the T-shaped well and the histogram of contrasts displays a clear bimodal distribution. Optical contrast is determined as $(I_p - I_b)/I_b$, where I_p and I_b denote electrostatic pixel and background intensities respectively. Displayed on the right are typical images of the ON (top) and OFF (bottom) states after subtraction of a reference OFF-state image. Scale bar represents 200 nm.

of the T (Fig. 3c). Working with polarized light and plasmonic nanorods, which display a strong polarization-dependent scattering response, we thus expect a bimodal optical readout of the trapped object's state in the double well.

To verify this model we employed commercially synthesized colloidal silver nanorods of nominal dimensions $160 \text{ nm} \times 50 \text{ nm}$ and an estimated net surface charge of about $-250 e$ per particle as the working element of the bistable system. Single nanorods trapped in individual potential wells are visualized by laser scanning microscopy using a linearly polarized illuminating optical probe field at $\lambda_p = 671 \text{ nm}$ lying within the broad longitudinal plasmon resonance of the nanorod^[33]. When trapped in wells with low barriers ($B \sim 10 k_B T$), and illuminated by a probe field polarized parallel to one arm of the well, trapped rods blink between bright and dark states on a timescale of seconds on account of thermal fluctuations between the two orthogonal orientations.

External control of a bistable colloid

The ability to actively manipulate the state of this bistable system using an external stimulus would open doors to harnessing nanometre-scale colloidal entities towards digital functionalities. To this end, we explore the response of our bistable rod to an external force and torque. A force applied to an object in a potential well biases its statistical behaviour: the free energy landscape tilts in the direction of the force. In a double-well potential a large

enough applied force could eliminate the barrier altogether and propel the object over into the neighbouring minimum. Here the particle may remain trapped even after the field is turned off, storing properties of the applied stimulus such as its magnitude and polarity. The barrier height at equilibrium determines the average lifetime of a written state, as well as the energy required to switch the object from one state to the next within a pre-defined time. E.g., an energy barrier of $30 k_B T$ in our system would imply an average lifetime in each state of about 30 years. Since the barrier height is in turn a function of a number of parameters, namely (i) the morphology of the potential well, (ii) net charge on the particle and walls, (iii) fluid properties (e.g., the mobile charge density and static permittivity) and (iv) particle dimensions, the system presents ample opportunity for tunability. In addition, the ability to actuate the colloidal bit by various stimuli electrical, hydrodynamic and optical presents a route to interface signals of different kinds, e.g., electro-optic or opto-mechanical signal transduction. In our original demonstration we use water as the suspending fluid (conductivity = $20 \mu\text{S}/\text{cm}$) and studied the behaviour of electrostatic pixels (i.e., a single rod in a bistable well) with barriers up to $40 k_B T$. Depending on the height of the barrier the pixel could be operated in two modes namely, volatile and non-volatile. While volatile operation is of interest for rapid modulation of states and sensing external fields, non-volatile operation enables information storage in a pixel-like memory element for future readout.

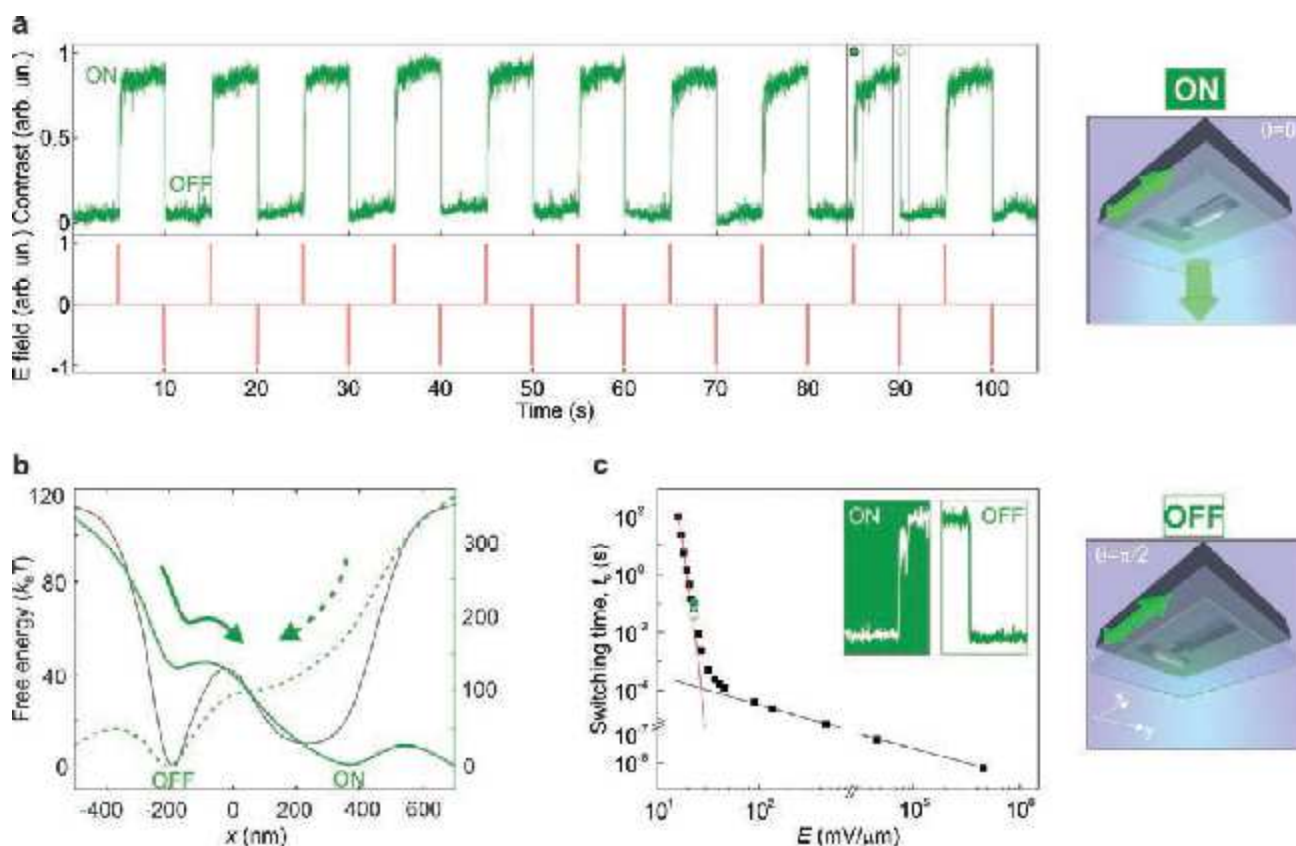


Fig. 4: Information storage in a rewriteable fluid-phase bit. (a) Measured normalized temporal optical contrast (green trace) for a nanorod trapped in the well depicted in Fig. 1b and driven by an alternating pulsatile electrical field ($|E| = 22.7 \text{ mV}/\mu\text{m}$) (red trace) of pulse width 0.2 s. (b) Line profiles of rod energy along $y = 0$, for external electrical fields, $E = 0$ (grey), $E = 22.7 \text{ mV}/\mu\text{m}$ (solid green) and $E = -22.7 \text{ mV}/\mu\text{m}$ (dashed green). (c) Brownian Dynamics simulation of switching time, for the OFF-ON transition of a single nanorod of charge $-250 e$ as a function of applied field (squares). The red line denotes a fit of the form $t_s \propto \exp(-cE)$ and represents the barrier-governed regime while the black line represents $t_s \propto 1/E$. Also displayed are experimentally measured switching times deduced from (a): OFF-ON transition ($\sim 100 \text{ ms}$, solid circle), ON-OFF transition ($\sim 40 \text{ ms}$, open circle). The former timescale slightly lags the latter due to a residual barrier between the states, evident from the green curves in (b).

To demonstrate the potential for data storage in our electro-optic bit, we focused on rods trapped in bistable wells with high barriers $B \sim 40 k_B T$ ($g = d = 100$ nm, $2h = 180$ nm) (Fig. 3b). As shown in Figs. 4a and b, application of a large pulsatile external field enables a particle to surmount the barrier, but unlike in volatile switching, the rod remains stably trapped in the new state with zero external field until the application of the next pulse. At ~ 0.7 pW/transition, the power required to switch a state is higher than in volatile operation, but in contrast, long-term storage of the written state is attained in a power-free fashion. A Brownian dynamics simulation of transport in a non-volatile pixel displays two distinct regimes of operation. In the limit of low applied fields the barrier between the two states decreases linearly with increasing field resulting in an exponential reduction of switching time, in keeping with Kramers theory (red line, Fig. 4c)^[17]. Thereafter, in the limit of large applied forces, the statistical component of transport disappears and the particle moves ballistically. For this system, the switching time t_s decomposes into two contributions, t_t and $t_{r,e}$. Here t_t represents lateral displacement between minima and $t_{r,e} \sim 90$ μ s the timescale on which the rod rotates to occupy the local angular electrostatic minimum. Although t_t can be reduced by increasing the applied field (Fig. 4c), in our current work t_s is limited by the speed of the process yielding the binary response – the rod's rotational relaxation.

Finally, we have also demonstrated control of light by light using our fluid-phase colloidal bit. An optical field that toggles the state of the nanorod not only presents a hardware-free route to switch actuation, but also enables all-optical gating of signals, and information storage and retrieval solely by means of light. Our strategy employed the ability of polarized light to impart angular momentum to optically anisotropic matter^[34-36]. Thus we replaced the external electric field with a linearly polarized, weakly focused Gaussian gate beam at $\lambda_g = 1064$ nm, red-detuned to the longitudinal resonance of the rod and applied in a pulsatile fashion. Due to symmetry considerations a single T-well however did not support reversible rod motion when driven by a torque. We therefore introduced a quadrastable potential created by an anti-parallel arrangement of two such wells and thereby converted the alternating linear momentum of the gate photons into an orbital angular motion of the particle.

These experiments demonstrated for the first time the feasibility of controlled spatial manipulation of a free-standing nanoscale entity on timescales approaching 10 μ s in optical control and 1 ms in electrical switching. The speed limit in electrical operation is defined by two processes, namely the electrical response time given by the system's RC constant, and the rise time of the fluid flow which depends on momentum diffusion. Conductance measurements place the former timescale at ~ 50 ns^[37], while the latter is well estimated by $h^2/\nu = 2.5$ ns for a 100 nm deep slit, where ν denotes the kinematic viscosity of water. Thus sub-microsecond response times are within reach of this scheme. Extrapolating from our measurements, individual switches actuated by local electrodes using e.g., voltages ~ 50 mV should yield switching times $t_s \approx 200$ μ s ($t_t \approx 200$ μ s) (Fig. 4c); this translates to an energy requirement of ~ 3 fJ per written state which we expect to increase as t_t^{-1} . The electrical energy requirement may however be significantly reduced to the limit given by frictional loss through the use of alternate slit

surface materials, putting the energy consumption on par with state-of-art data storage technologies. Finally we remark that our colloidal bit delivers transistor-like modulation in electrical operation, where less than a picowatt of electrical power could switch a milliwatt or more of optical power.

Dense arrays of addressable electrostatic pixels would have immediate implications for data storage, electrically or optically gated optical data transfer, high resolution displays^[38] as well as 2D adaptive optics or active metamaterial assemblies^[39]. A binary response driven by precise, reversible spatial transport of a nanoscale entity may be realized in a broad range of scenarios, e.g., modulation of the local density of optical states or radiation patterns, spectral tuning of object emission or nanostructure transmission^[40] (optical), break junction conductivity (electrical), or physical nanomechanical gates that regulate flow of fluids and/or charge carriers in fluidic conduits. This methodology may also provide a gateway to novel structural studies on biological macromolecules.

In the following section we discuss a new measurement principle and tool based on the electrostatic fluidic trap that enables for the first time highly precise measurements of the electrostatic properties of single macromolecules in solution.

MEASURING THE EFFECTIVE ELECTRICAL CHARGE AND INTERIOR DIELECTRIC CONSTANT OF SINGLE MACROMOLECULES

The electrostatic properties of macromolecules – specifically, their electrical charge and interior dielectric characteristics – are a vital component of their function, contributing to the physical basis of mechanisms ranging from molecular recognition, signaling and enzymatic catalysis, to protein folding and aggregation, and are of fundamental relevance in experiment and theory^[41-44]. The ability to perform a direct, sensitive, high-resolution measurement of the charge of a macromolecule in solution, and to relate the measurement to a suitable molecular structural model, would thus hold great importance from both a fundamental as well as a biomedical perspective.

At the simplest level a direct sum over a macromolecule's charged groups yields a qualitative estimate of its net electrical charge at a given solution pH,

$$q_{\text{str}} = \sum_i \frac{z_i e}{1 + 10^{z_i(pH - pK_i)}}, \quad (1)$$

where i denotes each ionizable group, pK_i is the negative logarithm of its acid dissociation constant, and $z_i = +1$ or -1 indicates a basic or an acidic group, respectively. In practice however, collective interactions in a densely packed system of charges can dramatically modify the molecule's effective charge in solution via two separate phenomena – namely, charge regulation and charge renormalization. The former concerns an alteration in the charged state of an ionizable group in the context of the molecular environment, while the latter deals with the highly non-linear screening of molecular charge by counterions in the surrounding electrolyte phase. Both phenomena generally result in a reduced effective charge of an electrically charged

object, and have received extensive theoretical attention, from polyelectrolytes and proteins to colloidal particles and charged surfaces in solution^[45-51].

We have achieved for the first time external field-free, stable trapping of biomolecules such as 10- 60 base oligonucleotides of ssDNA, dsDNA, intrinsically disordered proteins (IDPs) - Prothymosin α (ProT α , 10 kDa)^[52, 53] and Starmaker-like protein (Stm-I, 40 kDa)^[54], and a globular tetrameric enzyme, β -Glucuronidase (Gus β , 290 kDa) in aqueous solution. For example single Stm-I molecules can be trapped on time scales longer than half an hour. Note that in the reported experiments, the physical dimensions of the geometric perturbation that creates the trap (nanostructure depth and diameter, generally 200 - 600 nm) are much larger than the Debye length, $\kappa^{-1} \approx 10$ nm, the characteristic length scale of electrostatic interactions. As a result a molecule in a trap inhabits a region of zero electric field and zero electrical potential, and chemical equilibrium ensures that the solution conditions at the bottom of the potential well, where the molecule spends most of its time, are identical to those in the bulk solution.

Decreasing the depth of the potential well permits a transition from the regime of long-term trapping to short dwell times. Operating in this mode, we can, on time scales of ~ 100 ms to 1 second, accurately measure the average escape time, t_{esc} of a few molecules thermally sampling a high-density array of shallow traps. Crucially, t_{esc} depends exponentially on the molecule's solution-phase electrical charge, via a Kramers type expression

$$t_{\text{esc}} = t_r \exp\left\{\frac{W}{k_B T}\right\},$$

where t_r is a time scale that depends on the diffusivity of the molecule. We have found theoretically that W , the well depth depends predominantly on the product of the effective charge of the molecule, q and y_m , the mid-plane potential of the slit (unpublished work). The exponential dependence of the average escape time renders possible measurements of the charge of the molecule with a precision much better than the elementary charge, e . Since the average escape time can be determined with very high precision in a measurement of the kind described in Fig. 5, we were able to introduce the concept of escape from a potential well as a novel measurement principle that offers

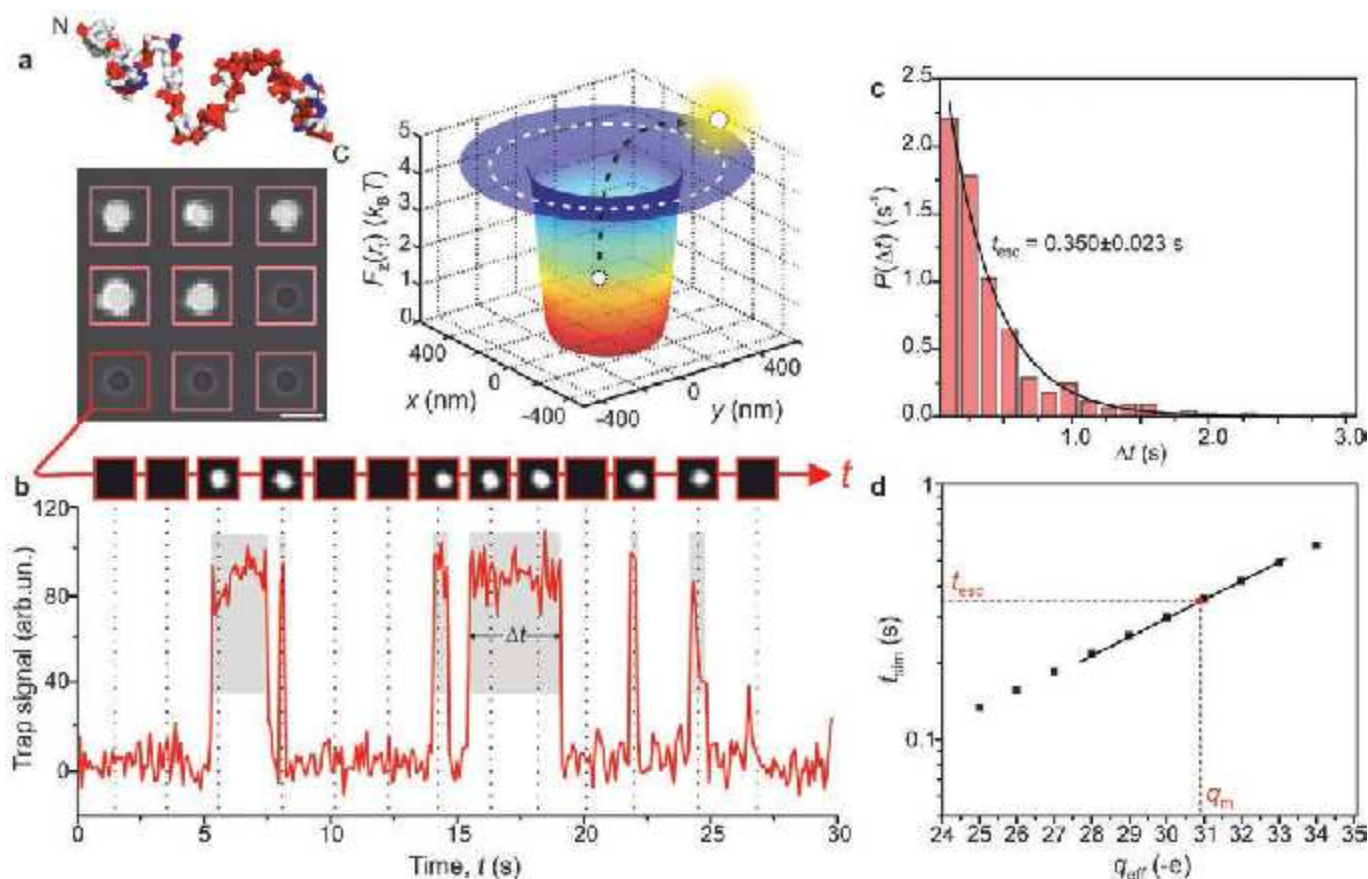


Fig. 5: Escape-time electrometry to determine the electrical charge of a trapped species. (a) A single snapshot of ProT α molecules each fluorescently labelled with two Atto 532 dye molecules sampling a 3x3 array of electrostatic fluidic traps (left) with slit height $2h = 76.4$ nm (scale bar $1 \mu\text{m}$). Shape of the inferred confining potential well (right). A series of snapshots of the array acquired using exposure time $t_{\text{exp}} = 30$ ms at a frequency of 33 Hz over a period of ca. 30 s is analyzed by recognising regions of interest defined by the locations of single traps (red squares) and monitoring the average intensity in the region as a function of time. A representative time trace of a single region-of-interest is depicted in (b). (b) The time traces are analyzed using a step-finding algorithm that identifies and determines the duration of residence of a molecule in a trap, Δt . (c) Residence- (escape-) time data recorded for ~ 10 -15 molecules ($N = 300$ escape events) is pooled and the normalised histogram fit with a single exponential of the form $P(\Delta t) = \frac{A}{t_{\text{esc}}} \exp\left\{-\frac{\Delta t}{t_{\text{esc}}}\right\}$, representing a Poisson process, where t_{esc} denotes the average measured escape time and $A \approx 1$. (d) 3D Brownian Dynamics simulation result of the average escape time, t_{esc} of a molecule as a function of its effective charge, q_{eff} (black symbols). The Brownian walk begins at the electrostatic potential minimum at $t_i = 0$ and the molecule is considered to have escaped the well when it traverses the dotted contour line in (a). The black line is a linear fit of the obtained t_{esc} vs. q_{eff} dependence, in the range of interest. In this case the measured $t_{\text{esc}} = 0.35 \pm 0.023$ s (red symbol) converts to a measured charge, $q_m = 30.9 \pm 0.4 e$.

major advantages over the previously described tracking-based approach to determining the charge of single colloidal particles in solution^[20]. We call the approach escape-time electrometry (ETe). Using the functional form of the spatial confining potential to determine the charge of a trapped object requires high signal-to-noise ratio (SNR) detection of the particle, with the experimentally measured quantity, e.g., a spring constant, depending at best linearly on the entity's charge. The escape-time approach on the other hand utilizes a telegraphic, on-off signal trace (Fig. 5b) and is ideally suited to the measurement of weak emitters, thus enabling the investigation of single molecules. Even more importantly, the approach offers rarely-attained exponential measurement sensitivity to the quantity of interest (Fig. 5d), and therefore renders possible charge measurements with unprecedented precision ($<1 e$). Measuring the effective charge of a molecule is independent of knowledge of

the molecule's composition or structure. Given a protein's amino acid composition however, we have shown that the measured charge can be used to infer the 3D distribution of charge in the molecule, as well as to estimate a dielectric coefficient of the molecular interior for folded molecules.

Fig. 6 compares our measured q_m values with the calculations of the effective charge, q_c , over a wide range of biomolecules. q_c is determined from free energy calculations^[19] that include the effects of both charge regulation and renormalization. For the disordered proteins and double stranded nucleic acids we find remarkable agreement between the measured and calculated charges, q_m and q_c , without any adjustable parameters. In contrast, for a compactly folded molecule such as a globular protein, we have to adjust the value of ϵ_p , a parameter representing the interior dielectric coefficient of a folded molecule,

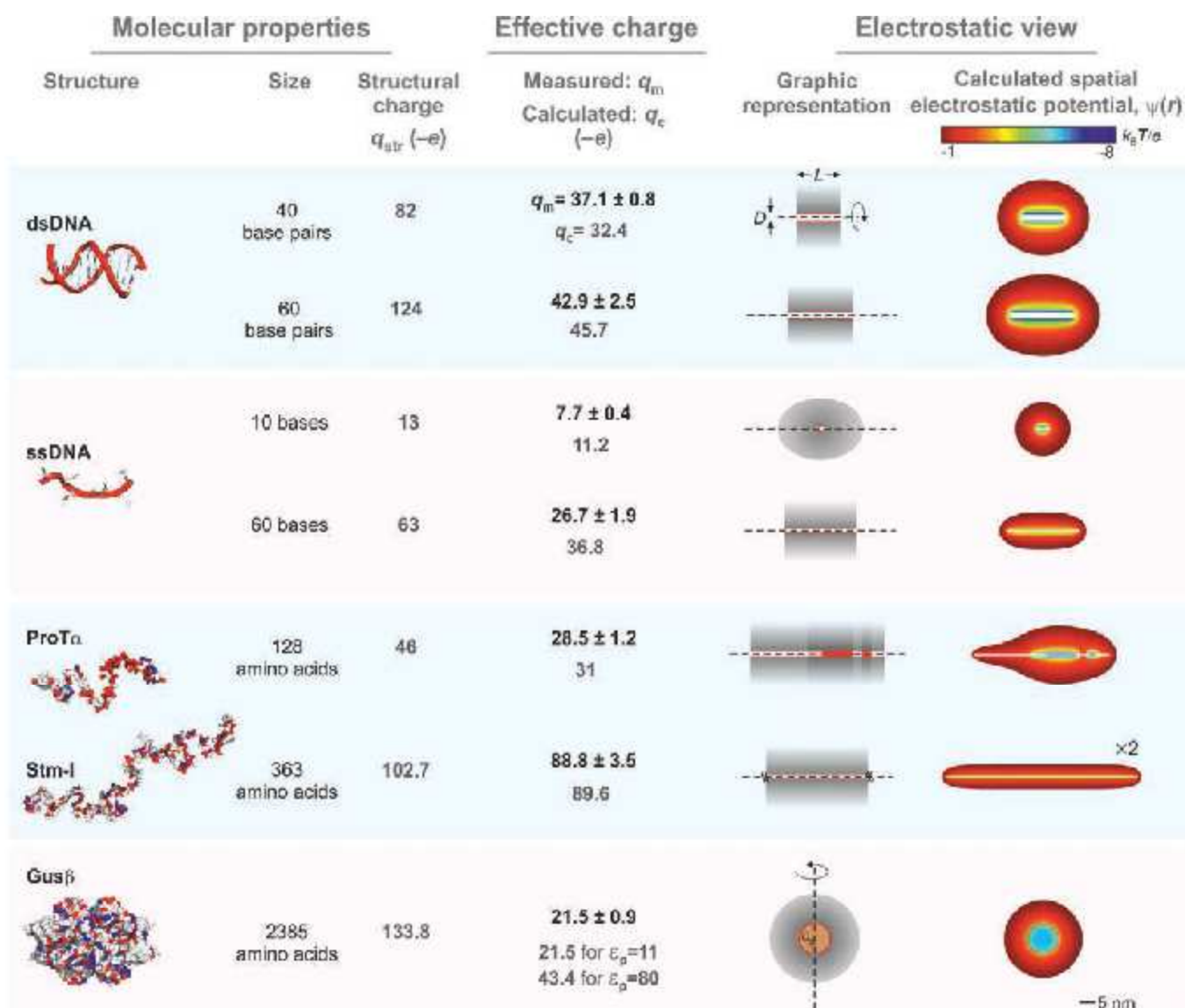


Fig. 6: The effective electrical charge of nucleic acids and proteins measured using escape-time electrometry. Columns from left to right: Structures of biomolecules as in Fig. 1c; Size of the molecule; Structural charge, q_{str} , calculated from equation (1), at the experimental pH, including the contribution of Atto 532 dye molecules; Effective electrical charge, both measured, q_m and calculated, q_c ; A molecular electrostatic view: Schematic representation of the modelled molecular geometry, with the dotted line denoting the axis of cylindrical symmetry, regions of net negative charge colored red and the spatial solution-phase counterion density in shades of grey (left), L and D denote the full contour length and diameter for the linear polyelectrolytes; Calculated spatial electrostatic potential distributions, $\psi(r)$ for each molecule, under the conditions of the measurement (right). Spatial scale for Stm-I is reduced by a factor 2. Note that the values for q_m denote averages over several independent measurements and the quoted errors are s.e.m.

to a value of around 11 in order to obtain agreement between measurement and theory (Fig. 6). Thus, observing the hopping dynamics of a single molecule in a well-determined free energy landscape should yield a wealth of information on its physical and structural properties.

Real time electrical charge measurements on one molecule

Finally, statistical considerations reveal that the measurement can indeed be performed on a single molecule in real time. Since escape from a potential well is a Poisson process and escape times are exponentially distributed, the fractional measurement uncertainty on t_{esc} from a sample of N statistically independent hops of a molecule is simply $N^{-1/2}$. For $N = 100$, the logarithmic dependence of q_m on t_{esc} implies $\sim 2\%$ precision in determining q_m . Speeding up the escape process so that $t_{\text{esc}} < 20$ ms and binning the entire time trace into consecutive blocks of $N = 2 - 100$ hops thus permits a real-time read out of the charge of a single molecule at a time resolution of ~ 20 ms 1 s with respective uncertainties on q_m of $\sim 20\% - 2\%$. Studying single 60 base ssDNA and ProT α molecules in this fashion

we demonstrated the ability to measure the effective charge of a single molecule in real time (Fig. 7). Comparing our measurements with simulations shows that the temporal charge fluctuations presented in Fig. 7c are largely statistical in origin. At the fundamental level the concept we propose would enable for the first time the observation of equilibrium effective charge fluctuations of a single molecule in solution, arising from e.g., reactions, interactions, or conformational changes.

Although at present our measurements are performed in a low salt environment (~ 2 mM), future experiments with optimized trap design and the use of alternate dielectrics or lipid bilayers as surface materials will enable charge measurements in the higher salt regime. Further, while the precision of our approach is already better than $1 e$, the accuracy of the method could be further improved by including a calibration molecule in the measurement whose charge is accurately known. One possibility would be a linear polyelectrolyte carrying a known number of ionizable groups spaced at a uniform distance, b significantly larger than the Bjerrum length, l_b . Doing so would circumvent residual

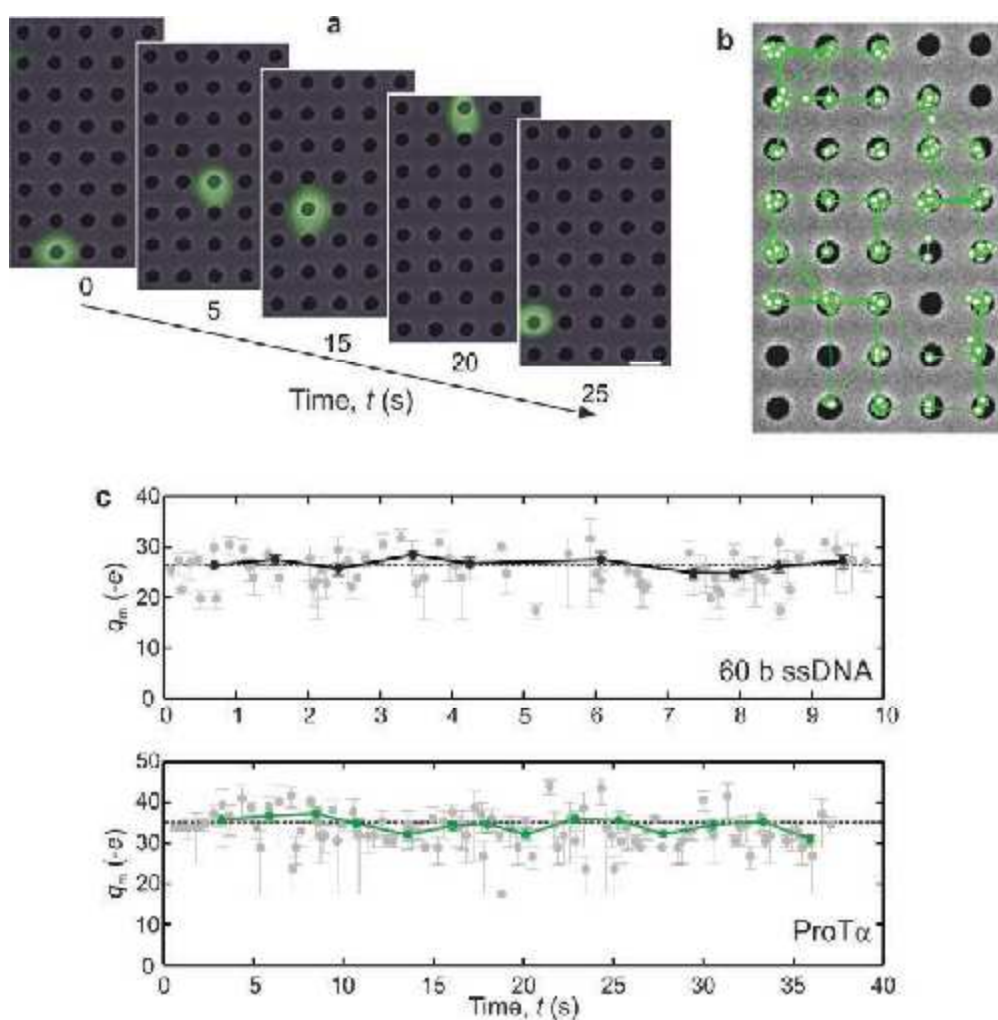


Fig. 7: Real-time measurement of the electrical charge of a single molecule. (a) Optical snapshots of a single 60 base ssDNA molecule (false color) sampling an array of traps, superimposed on an SEM of the trapping topography where the nanostructure diameter is 300 nm. (b) The trajectory of the molecule in time is used to generate its escape-time histogram. Scale bars denote 500 nm. (c) Binning a long single molecule trajectory into groups of $N = 3$ and 20 consecutive events yields real-time measurements of q_m at overall average temporal resolutions of ~ 150 ms (grey symbols) and ~ 1 s (black symbols) for ssDNA, and 370 ms (grey symbols) and 2.5 s (green symbols) for ProT α . Time-averaged q_m values are plotted as dashed lines in each case. All images were acquired using exposure times, $t_{\text{exp}} = 5$ ms; the experimental time scales were $t_{\text{esc},60b} = 34$ ms; $t_{\text{cycle}} \approx 5$ ms for 60 base ssDNA and $t_{\text{esc},\text{ProT}\alpha} = 72$ ms; $t_{\text{cycle}} = 25$ ms for ProT α . Note that for a given species the average q_m over all single molecules compares well with the ensemble measurements shown in Fig. 6. All error bars denote s.e.m.

uncertainties in slit height and salt concentration, and enable attainment of measurement accuracy approaching the precision given by the escape time measurement. It is also worth pointing out that the relatively low SNR~3 requirement of the method is ideally suited to the use of direct optical detection techniques e.g., scattering interferometry, which could in future obviate the need for chemical labeling of the molecule of interest^[55].

What the escape-time electrometry approach ultimately offers is the ability to perform a highly precise, real-time measurement of the electrical interaction energy of a single molecule in solution. We have shown that in conjunction with a theoretical model these measurements could provide for the first time a highly quantitative, systematic view of molecular electrostatics in solution. The dependence of the effective electrical charge of a biomolecule on its 3D conformation and our ability to sensitively measure small differences in charge immediately suggests a new physical observable to monitor a molecule's internal dynamics or folded state in real-time. Beyond the individual molecule these measurements can be readily applied to monitor intermolecular interactions, e.g., measuring binding free energies associated with molecular recognition^[56, 57]. In fact we envision developing a new family of experiments aimed at studying bimolecular and multimolecular interactions by confining two or more molecules in a trap. The development of a general approach to monitoring in real time the association and dissociation of two molecules engaged in a pair interaction, and measurement of the corresponding rates and free energies would have wide-ranging relevance e.g., in studies on the nucleation process, central to molecular aggregation and crystallization phenomena.

ACKNOWLEDGEMENTS

We gratefully acknowledge the support of the Swiss National Science Foundation and the University of Zurich.

REFERENCES

- [1] Chu, S. Cold atoms and quantum control. *Nature* **416**, 206-210 (2002).
- [2] Grier, D. G. A revolution in optical manipulation. *Nature* **424**, 810-816, doi:10.1038/nature01935 (2003).
- [3] Ashkin, A. Acceleration and trapping of particles by radiation pressure. *Phys. Rev. Lett.* **24**, 156-159 (1970).
- [4] Gosse, C. & Croquette, V. Magnetic tweezers: Micromanipulation and force measurement at the molecular level. *Biophys. J.* **82**, 3314-3329 (2002).
- [5] Chiou, P. Y., Ohta, A. T. & Wu, M. C. Massively parallel manipulation of single cells and microparticles using optical images. *Nature* **436**, 370-372, doi:10.1038/nature03831 (2005).
- [6] Soyka, F., Zvyagolskaya, O., Hertlein, C., Helden, L. & Bechinger, C. Critical Casimir Forces in Colloidal Suspensions on Chemically Patterned Surfaces. *Phys. Rev. Lett.* **101**, doi:10.1103/PhysRevLett.101.208301 (2008).
- [7] Cordovez, B., Psaltis, D. & Erickson, D. Electroactive micro and nanowells for optofluidic storage. *Optics Express* **17**, 21134-21148 (2009).
- [8] Cohen, A. E. & Moerner, W. E. Suppressing Brownian motion of individual biomolecules in solution. *Proc. Natl. Acad. Sci. U. S. A.* **103**, 4362-4365, doi:10.1073/pnas.0509976103 (2006).
- [9] Yang, A. H. J. et al. Optical manipulation of nanoparticles and biomolecules in sub-wavelength slot waveguides. *Nature* **457**, 71-75, doi:10.1038/nature07593 (2009).
- [10] Juan, M. L., Gordon, R., Pang, Y. J., Eftekhari, F. & Quidant, R. Self-induced back-action optical trapping of dielectric nanoparticles. *Nature Physics* **5**, 915-919, doi:10.1038/nphys1422 (2009).
- [11] Pang, Y. & Gordon, R. Optical Trapping of a Single Protein. *Nano Lett.* **12**, 402-406, doi:10.1021/nl203719v (2012).
- [12] Krishnan, M., Mojarad, N., Kukura, P. & Sandoghdar, V. Geometry-induced electrostatic trapping of nanometric objects in a fluid. *Nature* **467**, 692-695, doi:10.1038/nature09404 (2010).
- [13] Myers, C. J., Celebrano, M. & Krishnan, M. Information storage and retrieval in a single levitating colloidal particle. *Nature Nanotechnology* **10**, 886-891, doi:10.1038/nnano.2015.173 (2015).
- [14] Ruggeri, F., Zosel, F., Mutter, N., Różycka, M., Wojtas, M., Özyhar, A., Schuler, B. & Krishnan, M. Single-molecule electrometry. *Nature Nanotechnology*, doi:10.1038/NNANO.2017.26 (2017).
- [15] Behrens, S. H. & Grier, D. G. The charge of glass and silica surfaces. *J. Chem. Phys.* **115**, 6716-6721 (2001).
- [16] Israelachvili, J. N. *Intermolecular and surface forces*. 3rd edn, (Academic Press, 2011).
- [17] Kramers, H. A. Brownian motion in a field of force and the diffusion model of chemical reactions. *Physica* **7**, 284-304 (1940).
- [18] Kaplan, P. D., Faucheux, L. P. & Libchaber, A. J. Direct observation of the entropic potential in a binary suspension. *Phys. Rev. Lett.* **73**, 2793-2796 (1994).
- [19] Krishnan, M. Electrostatic free energy for a confined nanoscale object in a fluid. *J. Chem. Phys.* **138**, 114906, doi:10.1063/1.4795087 (2013).
- [20] Mojarad, N. & Krishnan, M. Measuring the size and charge of single nanoscale objects in solution using an electrostatic fluidic trap. *Nature Nanotechnology* **7**, 448-452, doi:10.1038/nnano.2012.99 (2012).
- [21] Jacobsen, V., Stoller, P., Brunner, C., Vogel, V. & Sandoghdar, V. Interferometric optical detection and tracking of very small gold nanoparticles at a water-glass interface. *Opt. Express* **14** (2006).
- [22] Wuttig, M. & Yamada, N. Phase-change materials for rewritable data storage. *Nature Materials* **6**, 824-832, doi:10.1038/nmat2009 (2007).
- [23] Waser, R. & Aono, M. Nanoionics-based resistive switching memories. *Nature Materials* **6**, 833-840, doi:10.1038/nmat2023 (2007).
- [24] Mahboob, I. & Yamaguchi, H. Bit storage and bit flip operations in an electromechanical oscillator. *Nature Nanotechnology* **3**, 275-279, doi:10.1038/nnano.2008.84 (2008).
- [25] Gittins, D. I., Bethell, D., Schiffrin, D. J. & Nichols, R. J. A nanometre-scale electronic switch consisting of a metal cluster and redox-addressable groups. *Nature* **408**, 67-69 (2000).
- [26] Loth, S., Baumann, S., Lutz, C. P., Eigler, D. M. & Heinrich, A. J. Bistability in atomic-scale antiferromagnets. *Science* **335**, 196-199, doi:10.1126/science.1214131 (2012).
- [27] Chen, W. et al. All-optical switch and transistor gated by one stored photon. *Science* **341**, 768-770, doi:10.1126/science.1238169 (2013).

- [28] Prakash, M. & Gershenfeld, N. Microfluidic bubble logic. *Science* **315**, 832-835, doi:10.1126/science.1136907 (2007).
- [29] Adleman, L. M. Molecular computation of solutions to combinatorial problems. *Science* **266**, 1021-1024, doi:10.1126/science.7973651 (1994).
- [30] Borshch, V., Shiyanovskii, S. V. & Lavrentovich, O. D. Nanosecond electro-optic switching of a liquid crystal. *Phys. Rev. Lett.* **111**, 107802, doi:10.1103/PhysRevLett.111.107802 (2013).
- [31] Kuzyk, A. et al. Reconfigurable 3D plasmonic metamolecules. *Nature Materials* **13**, 862-866, doi:10.1038/nmat4031 (2014).
- [32] De Silva, P. A., Gunaratne, N. H. Q. & McCoy, C. P. A molecular photoionic AND gate based on fluorescent signaling. *Nature* **364**, 42-44 (1993).
- [33] Celebrano, M., Rosman, C., Soennichsen, C. & Krishnan, M. Angular Trapping of Anisometric Nano-Objects in a Fluid. *Nano Lett.* **12**, 5791-5796, doi:10.1021/nl303099c (2012).
- [34] Ruijgrok, P. V., Verhart, N. R., Zijlstra, P., Tchegobtareva, A. L. & Orrit, M. Brownian fluctuations and heating of an optically aligned gold nanorod. *Phys. Rev. Lett.* **107**, 037401, doi:10.1103/PhysRevLett.107.037401 (2011).
- [35] Beth, R. A. Mechanical detection and measurement of the angular momentum of light. *Physical Review* **50**, 115-125, doi:10.1103/PhysRev.50.115 (1936).
- [36] Friese, M. E. J., Nieminen, T. A., Heckenberg, N. R. & Rubinsztein-Dunlop, H. Optical alignment and spinning of laser-trapped microscopic particles. *Nature* **394**, 348-350, doi:10.1038/28566 (1998).
- [37] Stein, D., Kruithof, M. & Dekker, C. Surface-charge-governed ion transport in nanofluidic channels. *Phys. Rev. Lett.* **93**, 035901, doi:10.1103/PhysRevLett.93.035901 (2004).
- [38] Zheng, G. et al. Metasurface holograms reaching 80% efficiency. *Nature Nanotechnology* **10**, 308-312 (2015).
- [39] Ou, J.-Y., Plum, E., Zhang, J. & Zheludev, N. I. An electromechanically reconfigurable plasmonic metamaterial operating in the near-infrared. *Nature Nanotechnology* **8**, 252-255, doi:10.1038/nnano.2013.25 (2013).
- [40] Shalin, A. S., Ginzburg, P., Belov, P. A., Kivshar, Y. S. & Zayats, A. V. Nano-opto-mechanical effects in plasmonic waveguides. *Laser & Photonics Reviews* **8**, 131-136, doi:10.1002/lpor.201300109 (2014).
- [41] Perutz, M. F. Electrostatic effects in proteins. *Science* **201**, 1187-1191, doi:10.1126/science.694508 (1978).
- [42] Warshel, A., Sharma, P. K., Kato, M. & Parson, W. W. Modeling electrostatic effects in proteins. *Biochimica et Biophysica Acta-Proteins and Proteomics* **1764**, 1647-1676, doi:10.1016/j.bbapap.2006.08.007 (2006).
- [43] Bah, A. et al. Folding of an intrinsically disordered protein by phosphorylation as a regulatory switch. *Nature* **519**, 106-109, doi:10.1038/nature13999 (2015).
- [44] Kamerlin, S. C. L., Sharma, P. K., Prasad, R. B. & Warshel, A. Why nature really chose phosphate. *Quarterly Reviews of Biophysics* **46**, 1-132, doi:10.1017/s0033583512000157 (2013).
- [45] Manning, G. S. Limiting laws and counterion condensation in polyelectrolyte solutions. I. Colligative properties. *Journal of Chemical Physics* **51**, 924-933, doi:10.1063/1.1672157 (1969).
- [46] Alexander, S. et al. Charge renormalization, osmotic-pressure, and bulk modulus of colloidal crystals - theory. *Journal of Chemical Physics* **80**, 5776-5781, doi:10.1063/1.446600 (1984).
- [47] Aubouy, M., Trizac, E. & Bocquet, L. Effective charge versus bare charge: an analytical estimate for colloids in the infinite dilution limit. *Journal of Physics a-Mathematical and General* **36**, 5835-5840, doi:10.1088/0305-4470/36/22/302 (2003).
- [48] Netz, R. R. & Orland, H. Variational charge renormalization in charged systems. *European Physical Journal E* **11**, 301-311, doi:10.1140/epje/i2002-10159-0 (2003).
- [49] Lund, M. & Jonsson, B. Charge regulation in biomolecular solution. *Quarterly Reviews of Biophysics* **46**, 265-281, doi:10.1017/s003358351300005x (2013).
- [50] Ninham, B. W. & Parsegian, V. A. Electrostatic potential between surfaces bearing ionizable groups in ionic equilibrium with physiologic saline solution. *Journal of Theoretical Biology* **31**, 405-428, doi:10.1016/0022-5193(71)90019-1 (1971).
- [51] Belloni, L. Ionic condensation and charge renormalization in colloidal suspensions. *Colloids and Surfaces a-Physicochemical and Engineering Aspects* **140**, 227-243, doi:10.1016/s0927-7757(97)00281-1 (1998).
- [52] Gast, K. et al. Prothymosin-alpha - a biologically-active protein with random coil conformation. *Biochemistry* **34**, 13211-13218, doi:10.1021/bi00040a037 (1995).
- [53] Mueller-Spaeth, S. et al. Charge interactions can dominate the dimensions of intrinsically disordered proteins. *Proc. Natl. Acad. Sci. U. S. A.* **107**, 14609-14614, doi:10.1073/pnas.1001743107 (2010).
- [54] Rozycka, M. et al. Intrinsically Disordered and Pliable Starmaker-Like Protein from Medaka (*Oryzias latipes*) Controls the Formation of Calcium Carbonate Crystals. *PLoS One* **9**, doi:10.1371/journal.pone.0114308 (2014).
- [55] Arroyo, J. O. et al. Label-Free, All-Optical Detection, Imaging, and Tracking of a Single Protein. *Nano Lett.* **14**, 2065-2070, doi:10.1021/nl500234t (2014).
- [56] Wang, Q. & Moerner, W. E. Single-molecule motions enable direct visualization of biomolecular interactions in solution. *Nat. Methods* **11**, 555-558, doi:10.1038/nmeth.2882 (2014).
- [57] Gao, J. M., Mammen, M. & Whitesides, G. M. Evaluating electrostatic contributions to binding with the use of protein charge ladders. *Science* **272**, 535-537, doi:10.1126/science.272.5261.535 (1996).